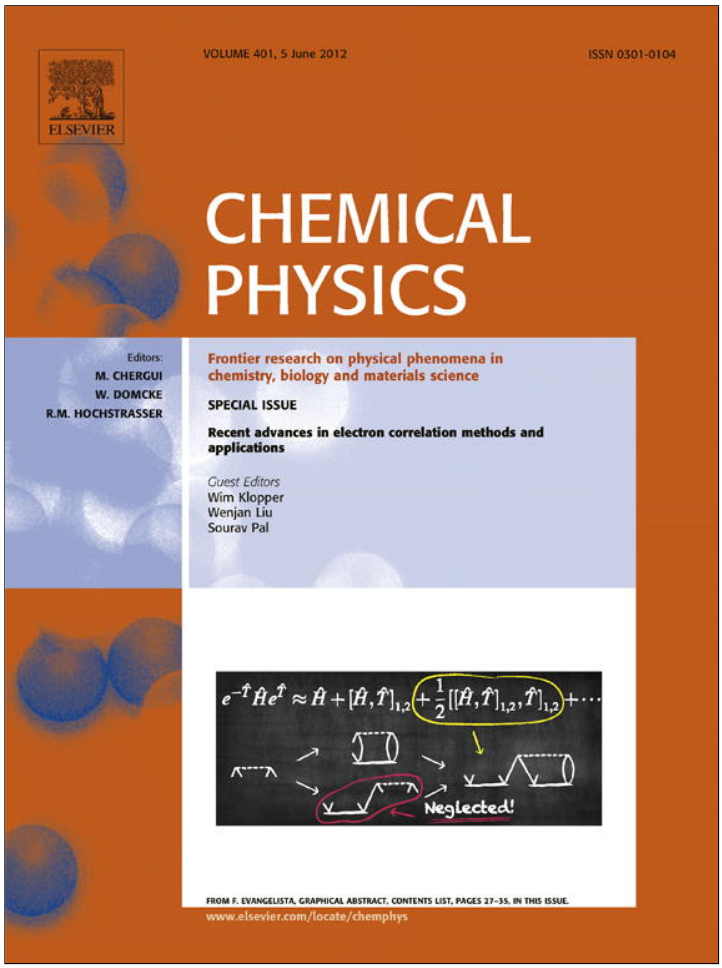
Provided for non-commercial research and education use.
Not for reproduction, distribution or commercial use.



This article appeared in a journal published by Elsevier. The attached copy is furnished to the author for internal non-commercial research and education use, including for instruction at the authors institution and sharing with colleagues.

Other uses, including reproduction and distribution, or selling or licensing copies, or posting to personal, institutional or third party websites are prohibited.

In most cases authors are permitted to post their version of the article (e.g. in Word or Tex form) to their personal website or institutional repository. Authors requiring further information regarding Elsevier's archiving and manuscript policies are encouraged to visit:

http://www.elsevier.com/copyright

Author's personal copy

Chemical Physics 401 (2012) 217–227

Contents lists available at SciVerse ScienceDirect

Chemical Physics

journal homepage: www.elsevier.com/locate/chemphys

Quartic scaling analytical gradients of scaled opposite-spin CC2

Nina O.C. Winter *, Christof Hättig

Lehrstuhl für Theoretische Chemie, Ruhr-Universität Bochum, 44801 Bochum, Germany

ARTICLE INFO

Article history:
Available online 21 October 2011

Dedicated to Prof. Dr. Debashis Mukherjee on the occasion of his 65th birthday.

Keywords:
Scaled opposite spin
CC2
ADC(2)
Excited state geometries

ABSTRACT

An implementation of analytical gradients, transition moments and excited state properties for scaled opposite-spin (SOS) CC2 and a SOS variant of the algebraic diagrammatic construction through second order ADC(2) is presented. The time-determining fifth order scaling steps in the algorithms are replaced by schemes with only fourth order scaling computational costs using a "resolution of the identity" approximation for the electron repulsion integrals and a numerical Laplace transformation of the orbital energy denominators. This leads to a significant reduction of the computational costs for geometry optimizations of large systems.

This work is an extension to the recently presented quartic scaling algorithm for SOS–CC2 energies for ground and excited states. The Laplace error for adiabatic electronic excitation energies and excited state structures is found to be very small. SOS–ADC(2) provides for adiabatic electronic excitation energies, excited state structure parameters, harmonic vibrational frequencies as well as dipole moments and transition strengths an accuracy similar to SOS–CC2. Timings for ground and excited state calculations are reported and applications to a chlorophyll molecule and a ditopic 2,2′:6′,2″-bis(terpyridine) with 160 atoms demonstrate how the new implementation extends the applicability of these methods for large systems.

© 2011 Elsevier B.V. All rights reserved.

1. Introduction

The determination of equilibrium geometries in electronically excited states is a challenging task in quantum chemistry. Geometry optimizations using numerical gradients suffer from a large computational effort and the numerical difficulties arising from the coordinate displacement. Analytical gradients are therefore necessary for a fast and reliable calculation of equilibrium structures in ground and electronically excited states. Vibrational frequencies can then be obtained by numerical differentiation of the analytical gradients. Thereby adiabatic electronic excitation energies and 0–0 transition energies are available. Transition moments and excited state properties as e.g. dipole or quadrupole moments can be used to further characterize electronic transitions.

CC2 is a coupled cluster method, for which these properties can be derived in a straightforward manner using the framework of response theory [1–4]. Unfortunately conventional CC2 is a quite expensive method as its computational costs increase with fifth order of the system size. For a scaled opposite spin (SOS) ansatz of MP2 gradients a quartic scaling implementation was presented by Lochan et al. [5]. Fourth order scaling gradient calculations for excited states were reported for SOS-CIS(D_0) [6].

SOS–CC2 provides an accuracy comparable to unscaled CC2 for equilibrium bond distances and adiabatic electronic excitation energies [7]. A scaled opposite spin (SOS) ansatz for CC2 can be implemented with only fourth order scaling computational costs using the resolution-of-the-identity (RI) approximation for the electron repulsion integrals and a numerical Laplace transformation of the orbital energy denominators. A numerical Laplace transformation is also used in local CC2 response methods [8,9], which are available for excitation energies, transition moments and first-order properties. Here we extended the recently presented fourth order scaling algorithm for SOS–CC2 energies [10] to the calculation of first-order properties and gradients for ground and excited states as well as transition moments. A quartic scaling algorithm for gradients of a SOS variant of the algebraic diagrammatic construction through second order ADC(2), which is a cost-efficient alternative to SOS–CC2, is also presented.

In Section 2 the theoretical background of SOS–CC2 gradient theory is briefly described, where the focus is on the time-determining steps of the algorithms. In Section 3 the implementation of the algorithms in the TURBOMOLE program package [11] is presented. In Section 4.1 the errors for adiabatic electronic excitation energies and structures in the excited state arising from the numerical Laplace transformation are investigated. In Section 4.2 the accuracy of SOS–ADC(2) for adiabatic excitation energies, excited state structures, harmonic vibrational frequencies as well as dipole moments and transition strengths is evaluated and

* Corresponding author. Tel.: +49 234 3224523; fax: +49 234 3214045.
E-mail addresses: Nina.Winter@theochem.rub.de (N.O.C. Winter), Christof.Haettig@rub.de (C. Hättig).

0301-0104/$ - see front matter © 2011 Elsevier B.V. All rights reserved.
doi:10.1016/j.chemphys.2011.10.002

Author's personal copy

compared to SOS–CC2 and unscaled CC2. In Sections 4.3 and 4.4 the efficiency of the fourth order scaling implementation is demonstrated using two large molecules, chlorophyll and a ditopic 2,2′:6′,2″-bis(terpyridine), as examples.

2. Theory

The SOS–CC2 [7] ground state energy is given by

$$E_{\mathrm{SOS}} = \langle \mathrm{HF}|\widetilde{\widehat{H}} + c_{\mathrm{os}}\left[\widetilde{\widehat{H}}, \widehat{T}_2^{\mathrm{os}}\right]|\mathrm{HF}\rangle, \tag{1}$$

with the amplitudes determined by the cluster equations:

$$\Omega_{\mu_1} = \langle \mu_1|\widetilde{\widehat{H}} + c_{\mathrm{os}}\left[\widetilde{\widehat{H}}, \widehat{T}_2^{\mathrm{os}}\right]|\mathrm{HF}\rangle = 0, \tag{2}$$

$$\Omega_{\mu_2} = \langle \mu_2^{\mathrm{os}}|\widetilde{\widehat{H}} + \left[\widehat{F}, \widehat{T}_2^{\mathrm{os}}\right]|\mathrm{HF}\rangle = 0. \tag{3}$$

In the latter equations $\widetilde{\widehat{H}}$ denotes the similarity-transformed Hamiltonian $\widehat{H} = e^{-\hat{T}_1}\widehat{H}e^{\hat{T}_1}$. The spin scaling is realized by using the two-electron excitation operator $\widehat{T}_2^{\mathrm{os}}$, which acts only on two electrons with different spins. μ_1 are singly excited determinants and μ_2^{os} are doubly excited determinants generated from the excitations included in $\widehat{T}_2^{\mathrm{os}}$. For the scaling factor we use $c_{\mathrm{os}} = 1.3$, which is the same factor as optimized by Jung et al. for SOS-MP2 [12].

As described in Ref. [13], excitation energies are derived as eigenvalues of the SOS–CC2 Jacobi matrix **A** with $A_{\mu_i\nu_j} = \frac{\partial \Omega_{\mu_i}}{\partial t_{\nu_j}}$. For the total energy of an excited state a Lagrange functional [2] can be constructed as:

$$L^{ex}_{\mathrm{SOS-CC2}} = E_{\mathrm{SOS}} + \sum_{ij=1}^{2}\sum_{\mu_i\nu_j}\bar{E}_{\mu_i}A_{\mu_i\nu_j}E_{\nu_j} + \bar{\omega}\left(1 - \sum_{i=1}^{2}\sum_{\mu_i}\bar{E}_{\mu_i}E_{\mu_i}\right) + \sum_{i=1}^{2}\sum_{\mu_i}\bar{t}^{ex}_{\mu_i}\Omega_{\mu_i} + \sum_{\mu_0}\bar{\kappa}^{ex}_{\mu_0}F_{\mu_0}, \tag{4}$$

where E_{SOS} and Ω_{μ_i} are given in Eqs. (1)–(3). E_{μ_i} is the right and $\bar{E}_{\mu_i}$ the left eigenvector of the SOS–CC2 Jacobi matrix, $\bar{t}_{\mu_i}$ are the Lagrange multipliers for the cluster equations and $\bar{\kappa}_{\mu_0}$ are Lagrange multipliers for the orbital rotations. The second term in Eq. (4) accounts for the transition energy from the ground to the excited state and the third term ensures that E_{μ_i} and $\bar{E}_{\mu_i}$ are bi-orthonormal. If we skip these two terms this leads us to the CC2 ground state Lagrange functional [1].

In the following we make use of the resolution-of-the-identity (RI) approximation [14] for the four-index electron repulsion integrals (ERIs):

$$(pq|rs)^{RI} = \sum_P B^P_{pq}B^P_{rs}, \tag{5}$$

with the three-index intermediates:

$$B^P_{pq} = \sum_{\alpha\beta Q} C_{\alpha p}C_{\beta q}(\alpha\beta|Q)[V^{-1/2}]_{QP}. \tag{6}$$

Here and in the following we use the convention that p, q, r, s are MO indices, α, β are AO indices and P, Q are auxiliary functions for the RI approximation. The integrals $(\alpha\beta|Q)$ are three-index ERIs, $V_{QP} = (Q|P)$ are two-index ERIs and **C** is the usual MO coefficient matrix.

Introducing unrelaxed one- and two-particle densities D_{pq} and $\hat{d}^{nsep}_{pqrs}$ as defined in Ref. [2], we can express Eq. (4) as:

$$L^{ex}_{\mathrm{SOS-CC2}} = \langle \mathrm{HF}|H|\mathrm{HF}\rangle + \sum_{pq}\left(D^{F,\xi}_{pq}(\bar{t}^{ex}) + D^{F,A}_{pq}(\bar{E},E)\right)F_{pq} + \frac{1}{2}\times\sum_{pqrs}\left(\hat{d}^{nsep,\xi}_{pqrs}(\bar{t}^{ex}) + \hat{d}^{nsep,A}_{pqrs}(\bar{E},E)\right)(pq|\widehat{rs})^{RI} + \bar{\omega}\left(1 - \sum_{i=1}^{2}\sum_{\mu}\bar{E}_{\mu_i}E_{\mu_i}\right) + \sum_{\mu_0}\bar{\kappa}^{ex}_{\mu_0}F_{\mu_0}. \tag{7}$$

The caret on the two-electron integrals and densities indicates that these quantities refer to the t_1-similarity transformed basis. The modified four-index ERIs are efficiently obtained as:

$$(pq|\widehat{rs})^{RI} = \sum_P \widehat{B}^P_{pq}\widehat{B}^P_{rs}, \tag{8}$$

where the three-index intermediates:

$$\widehat{B}^P_{pq} = \sum_{\alpha\beta Q}\Lambda^p_{\alpha p}\Lambda^h_{\beta q}(\alpha\beta|Q)\left[V^{-1/2}\right]_{QP} \tag{9}$$

are calculated with transformation matrices $\Lambda^p = \mathbf{C}(1 - t_1^T)$ and $\Lambda^h = \mathbf{C}(1 + t_1)$.

The densities for the ground state Lagrangian can be obtained as $D^{gs}_{pq} = D^{F,\xi}_{pq}(\bar{t}^{gs})$ and $\hat{d}^{nsep,gs}_{pqrs} = \hat{d}^{nsep,\xi}_{pqrs}(\bar{t}^{gs})$ i.e., by replacing the Lagrangian multipliers $\bar{t}^{ex}$ by $\bar{t}^{gs}$, whereas $D^{F,A}_{pq}$ and $\hat{d}^{nsep,A}_{pqrs}$ have no counterparts in the ground state Lagrangian. To calculate one-photon transition strengths [3]:

$$S^{0f}_{V_1V_2} = \frac{1}{2}\left\{M^{V_1}_{0\leftarrow f}M^{V_2}_{f\leftarrow 0} + \left(M^{V_2}_{0\leftarrow f}M^{V_1}_{f\leftarrow 0}\right)^*\right\}, \tag{10}$$

the "left" $\left(M^V_{0\leftarrow f}\right)$ and "right" $\left(M^V_{f\leftarrow 0}\right)$ transition moments:

$$M^V_{0\leftarrow f} = \left[D^{\eta}_{pq}(E) + D^{\xi}_{pq}(\overline{M})\right]\widehat{V}_{pq}, \tag{11}$$

$$M^V_{f\leftarrow 0} = D^{\xi}_{pq}(\bar{E})\widehat{V}_{pq} \tag{12}$$

have to be computed, where $\overline{M}$ are the transition moment Lagrangian multipliers [15] and $\widehat{V} = e^{-\hat{T}_1}Ve^{\hat{T}_1}$ is the similarity-transformed operator for the interaction with the electromagnetic field, e.g., the dipole operator. Explicit expressions for the one-particle density D^{η}_{pq} are given in Ref. [4].

In the conventional algorithm fifth order scaling steps appear during the solution of the left and right eigenvalue problem, the determination of the Lagrange multipliers $\bar{t}, \overline{M}$ and the calculation of the one- and two-particle densities D_{pq} and $\hat{d}^{nsep}_{pqrs}$. In our previous work [10] we described a fourth order scaling algorithm for the solution of the right eigenvalue problem. The time-determining steps in the calculation of the left eigenvectors $\bar{E}$ and the Lagrange multipliers $\bar{t}$ and $\overline{M}$ are similar to the solution of the right eigenvalue problem [4,1,2]. Therefore we will only discuss the computation of the one- and two-particle densities in the following. To reduce the storage requirements and the operation count for gradient calculations, the non-separable two-particle densities $\hat{d}^{nsep}_{pqrs}$ are contracted with three-index integrals to the three-index intermediates:

$$\Delta^P_{pq} = \sum_{rs}\hat{d}^{nsep}_{pqrs}\widehat{B}^P_{rs}. \tag{13}$$

The calculation of Δ^P_{pq} requires intermediates, which are similar to the three-index intermediates Y^P_{ai} used during the solution of the eigenvalue problem. Only the doubles contribution to the one-particle densities D_{pq} requires a new strategy to get to a fourth order scaling algorithm, which is illustrated in detail in Section 3.1.

The equations for SOS–ADC(2) excitation energies and excited state first-order properties and gradients can be derived from the SOS–CC2 expressions by neglecting the singles part of the ground state cluster amplitudes t_1 and symmetrizing the Jacobi matrix [10]. The ground state amplitudes reduce then to the scaled opposite-spin first-order amplitudes (in the sense of a scaled opposite-

Author's personal copy

spin perturbation theory [16]) and the eigenvalue problem is symmetric, i.e. left and right eigenvectors are identical. Consistent with this, the SOS-MP2 ground state energy is added to the SOS–ADC(2) excitation energies to get total energies for the excited states. Thus, for SOS–ADC(2) fewer equations for the eigenvectors and no iterative equations for the ground state amplitudes or the Lagrange multipliers $\bar{t}^{ex}$ need to be solved. Apart from that the derivation of the one-particle densities for the excited state gradient and first-order properties is completely analogous to CC2 [17].

The expressions for the transition moments of the strict ADC(2) model, as given in Ref. [18], are, as the energy, complete through second order in the electron fluctuation potential but require the second-order ground state single and double excitation amplitudes (i.e., the amplitudes from which the MP4(SDQ) energy can be calculated). The costs for computing the second-order doubles amplitudes scale as $\mathcal{O}(\mathcal{N}^6)$ and are incommensurate with the size of molecules for which RI-ADC(2) and SOS–ADC(2) are usually applied. Spectral intensities are usually not needed with a high accuracy and their accuracy is anyway limited by the accuracy of the eigenvector, which describes the excited state. In the RI-ADC(2) implementation of the TURBOMOLE program package we neglect therefore contributions, which are second-order in the ground state amplitudes, in the calculation of transition densities. This is justified by the fact that already terms first-order in the ground state amplitudes are small. In this work the same approximation is applied for SOS–ADC(2), e.g. contributions, which are second-order in the SOS ground state amplitudes, are neglected. With this approximation the transition strengths are still correct through the same order in perturbation theory as for the corresponding CC2 approaches and the results are indeed very similar, if there are no significant differences in the eigenvectors. Therewith the computation of transition densities for ADC(2) and SOS–ADC(2) is – similar to the computation of gradients – considerably cheaper than for the corresponding CC2 approaches because fewer equations need to be solved.

3. Implementation

3.1. Ground state one-particle density

In the following we demonstrate the derivation of a fourth order scaling algorithm for the one-particle densities using the example of the ground state density for SOS–CC2. Detailed expressions for $D^{F,\xi}_{pq}(\bar{t}^{gs})$ and the three-index intermediate Δ^{P}_{pq} from the corresponding two-particle density have been presented in Ref. [1]. As they remain (apart from the spin-scaling of the amplitudes) unchanged for SOS–CC2, we do not repeat them here. Doubles contributions to $D^{F,\xi}_{pq}(\bar{t})$ enter through the intermediates:

$$P^{\xi}_{ij} = -c_{os}\sum_{abk}\bar{t}_{ajbk}t_{aibk}, \tag{14}$$

$$P^{\xi}_{ab} = c_{os}\sum_{ijc}\bar{t}_{aicj}t_{bicj}, \tag{15}$$

$$C_{ai} = c_{os}\sum_{bj}t_{aibj}\bar{t}_{bj}. \tag{16}$$

The Lagrange multipliers $\bar{t}^{gs}$ for the ground state are given by

$$\bar{t}^{gs}_{aibj} = -\frac{(ai|\breve{bj})^{RI}}{\epsilon_a-\epsilon_i+\epsilon_b-\epsilon_j}, \tag{17}$$

where the modified four-index ERIs are obtained as:

$$(ai|\breve{bj})^{RI} = S^{ab}_{ij}\left(\sum_{P}B^{P}_{ai}\left(B^{P}_{bj}+\breve{B}^{P}_{bj}\right)+\widehat{F}_{ia}\bar{t}_{bj}\right). \tag{18}$$

In the last equation the three-index intermediates:

$$\breve{B}^{P}_{pq} = \sum_{\alpha\beta Q}\left(\breve{\Lambda}^{p}_{\alpha p}\Lambda^{h}_{\beta q}+\Lambda^{p}_{\alpha p}\breve{\Lambda}^{h}_{\beta q}\right)(\alpha\beta|Q)\left[V^{-1/2}\right]_{Qp} \tag{19}$$

are evaluated with transformation matrices $\breve{\Lambda}^{p}=\Lambda^{p}\bar{t}_1$ and $\breve{\Lambda}^{h}=\Lambda^{h}\bar{t}^{T}_1.S^{ab}_{ij}$ is a symmetrization operator: $S^{ab}_{ij}\left(B^{P}_{ai}\breve{B}^{P}_{bj}\right)=B^{P}_{ai}\breve{B}^{P}_{bj}+\breve{B}^{P}_{ai}B^{P}_{bj}$ and $\widehat{F}$ is a Fock matrix calculated from the similarity-transformed Hamiltonian $\widetilde{\widehat{H}}=e^{-\widehat{T}_1}\widehat{H}e^{\widehat{T}_1}$ [4].

The cluster amplitudes are obtained as:

$$t_{aibj} = -\frac{(ai|\widehat{bj})^{RI}}{\epsilon_a-\epsilon_i+\epsilon_b-\epsilon_j}, \tag{20}$$

where $(ai|\widehat{bj})^{RI}$ was introduced in Eq. (8). With Eqs. (17) and (20) we can express the intermediate in Eq. (14) as:

$$P^{\xi}_{ij} = -c_{os}\frac{1}{\epsilon_i-\epsilon_j}\times\sum_{abk}\left(\frac{1}{\epsilon_a-\epsilon_i+\epsilon_b-\epsilon_k}-\frac{1}{\epsilon_a-\epsilon_j+\epsilon_b-\epsilon_k}\right)(a\breve{j}|bk)^{RI}(ai|\widehat{bk})^{RI}. \tag{21}$$

To decompose the orbital energy denominators $\frac{1}{\epsilon_{aibj}}$ with $\epsilon_{aibj}=\epsilon_a-\epsilon_i+\epsilon_b-\epsilon_j$ of the doubles contribution a numerical Laplace transformation [19–21] is used:

$$\frac{1}{\epsilon_{aibj}} = \int_0^{\infty}e^{-\epsilon_{aibj}t}dt \approx \sum_{z}^{n}w_z e^{-\epsilon_{aibj}t_z}. \tag{22}$$

Here w_z are the weights and t_z the grid points of the numerical quadrature procedure. With this approximation Eq. (21) can be rewritten as:

$$P^{\xi}_{ij} = -c_{os}\sum_{z}w_z\left(\frac{e^{\epsilon_i t_z}-e^{\epsilon_j t_z}}{\epsilon_i-\epsilon_j}\sum_{abk}(a\breve{j}|bk)^{RI}(ai|\widehat{bk})^{RI}e^{-(\epsilon_a+\epsilon_b-\epsilon_k)t_z}\right). \tag{23}$$

The prefactor of the summation over a, b and k can be reformulated as:

$$g^{z}_{ij} = \frac{e^{\epsilon_i t_z}-e^{\epsilon_j t_z}}{\epsilon_i-\epsilon_j} = t_z e^{(\epsilon_i+\epsilon_j)t_z/2}\frac{\sinh\left[(\epsilon_i-\epsilon_j)t_z/2\right]}{(\epsilon_i-\epsilon_j)t_z/2}, \tag{24}$$

where numerical instabilities in the case of near degenerate orbitals are avoided by the continuity of g^{z}_{ij} at the limit $\epsilon_i\approx\epsilon_j$ as described in Ref. [21].

Using the RI expressions for the four-index ERIs P_{ij} can be evaluated as:

$$P^{\xi}_{ij} = -\sum_{Qaz}g^{z}_{ij}\,\breve{Y}^{Q}_{aiz}\widehat{B}^{Q}_{aj}\cdot e^{-\epsilon_a t_z}, \tag{25}$$

where

$$\breve{Y}^{Q}_{aiz} = -c_{os}w_z\sum_{P}\left(N^{QP}_{z}\left(B^{P}_{ai}+\breve{B}^{P}_{ai}\right)+\breve{N}^{QP}_{z}B^{P}_{ai}\right)+n^{Q}_{z}\bar{t}_{ai}+\breve{n}^{Q}_{z}\widehat{F}_{ia}. \tag{26}$$

The intermediates used in the last equation are defined as:

$$N^{QP}_{z} = \sum_{bj}B^{P}_{bj}\widehat{B}^{Q}_{bj}e^{-(\epsilon_b-\epsilon_j)t_z}, \tag{27}$$

$$\breve{N}^{QP}_{z} = \sum_{bj}(B^{P}_{bj}+\breve{B}^{P}_{bj})\widehat{B}^{Q}_{bj}e^{-(\epsilon_b-\epsilon_j)t_z}, \tag{28}$$

$$n^{Q}_{z} = \sum_{bj}\widehat{F}_{jb}\widehat{B}^{Q}_{bj}e^{-(\epsilon_b-\epsilon_j)t_z}, \tag{29}$$

$$\breve{n}^{Q}_{z} = \sum_{bj}\bar{t}_{bj}\widehat{B}^{Q}_{bj}e^{-(\epsilon_b-\epsilon_j)t_z}. \tag{30}$$

Author's personal copy

With $\breve{Y}^Q_{aiz}$ also the virtual/virtual block P^ξ_{ab} can be calculated as:

$$P^\xi_{ab} = \sum_{Qiz} g^z_{ab} \breve{Y}^Q_{aiz} \hat{B}^Q_{bi} \cdot e^{\epsilon_i t_z} \tag{31}$$

with [21]:

$$g^z_{ab} = -\frac{e^{-\epsilon_a t_z} - e^{-\epsilon_b t_z}}{\epsilon_a - \epsilon_b} = t_z e^{-(\epsilon_a+\epsilon_b)t_z/2} \frac{\sinh\left[(\epsilon_a - \epsilon_b)t_z/2\right]}{(\epsilon_a - \epsilon_b)t_z/2}. \tag{32}$$

The remaining doubles contribution to $D^{F,\xi}_{pq}$ is easily obtained by

$$C_{ai} = -c_{os} \sum_{Qz} w_z \breve{n}^Q_z \hat{B}^Q_{bj} e^{-(\epsilon_b - \epsilon_j)t_z}. \tag{33}$$

Please note that $\breve{Y}^Q_{aiz}$ in Eq. (26) still depends on the Laplace quadrature points. For the calculation of the two-particle density Δ^P_{pq} an intermediate $\breve{Y}^Q_{ai}(\bar{t}^{gs}) = c_{os}\sum_{bj} \bar{t}^{gs}_{aibj} \hat{B}^Q_{bj}$ is needed, which is independent of the quadrature points. This can be obtained from $\breve{Y}^Q_{aiz}$ as:

$$\breve{Y}^Q_{ai}(\bar{t}^{gs}) = \sum_z \breve{Y}^Q_{aiz} e^{-(\epsilon_a - \epsilon_i)t_z}. \tag{34}$$

To replace all fifth order scaling steps in the computation of Δ^P_{pq} we evaluate in addition $\widetilde{Y}^Q_{ai}(t) = c_{os}\sum_{bj} t_{aibj} \breve{B}^P_{bj}$ with a fourth order scaling algorithm. This is achieved by calculating it as:

$$\widetilde{Y}^P_{ai}(t) = -c_{os} \sum_{Qz} w_z \breve{N}^{PQ}_z \hat{B}^Q_{ai} e^{-(\epsilon_a - \epsilon_i)t_z}. \tag{35}$$

As no t_z-dependent analog of $\widetilde{Y}^Q_{ai}$ is needed for the calculation of $D^{F,\xi}_{pq}(\bar{t})$ the summation over the quadrature points is carried out already in Eq. (35). All other contributions to the ground state one- and two-particle densities are obtained as described in Ref. [1] with operation counts scaling at most quartic with the system size.

3.2. Excited state one-particle densities

For the excited state gradient the one-particle density $D^{F,\xi}_{pq}(\bar{t}^{ex})$ calculated from the excited state Lagrange multipliers $\bar{t}^{ex}$ is needed (see Eq. (7)). The doubles part of these Lagrangian multipliers:

$$\bar{t}^{ex}_{aibj} = -\frac{S^{ab}_{ij}\left(\sum_P B^P_{ai}\left(B^P_{bj} + \breve{B}^P_{bj} + \bar{\breve{B}}^P_{bj}\right) + \hat{F}_{ia}\bar{t}_{bj} + \bar{F}_{ia}\bar{E}_{bj}\right)}{\epsilon_a - \epsilon_i + \epsilon_b - \epsilon_j}, \tag{36}$$

contains additional singles contributions originating from the left eigenvector $\bar{E}$ and a Fock matrix $\bar{F}$, which is calculated from the modified Hamiltonian $\bar{\hat{H}} = \left[\hat{\bar{H}}, \hat{E}_1\right]$, where $\hat{E}_1$ is the singles part of a cluster operator built with amplitudes from the right eigenvector. The intermediates $\breve{B}^P_{bj}$ depend on the singles part of the excited state Lagrange multipliers $\bar{t}^{ex}_1$ in this context and the intermediate:

$$\bar{\breve{B}}^Q_{ai} = -\sum_k \left(\sum_c \bar{E}_{ci}E_{ck}\right) B^Q_{ak} - \sum_c \left(\sum_k \bar{E}_{ak}E_{ck}\right) B^Q_{ci} \tag{37}$$

is calculated from the singles part of the left and right eigenvectors $\bar{E}$ and E. The fourth order scaling algorithm for $D^{F,\xi}_{pq}(\bar{t}^{ex})$ can thus be derived in the same way as for $D^{F,\xi}_{pq}(\bar{t}^{gs})$. The only difference is that in the calculation of $\breve{Y}^Q_{aiz}$ two additional n^Q_z intermediates have to be included, which account for the contributions of $\bar{E}$ and $\bar{F}$.

Excited state gradient and first-order property calculation additionally require the one-particle density $D^{F,A}_{pq}(\bar{E}, E)$ (see Eq. (7)). The doubles contributions to $D^{F,A}_{pq}(\bar{E}, E)$ are: [2]

$$P^A_{ij} = -c_{os} \sum_{abk} \bar{E}_{aibk}E_{ajbk}, \tag{38}$$

$$P^A_{ab} = c_{os} \sum_{ijc} \bar{E}_{aicj}E_{bicj}, \tag{39}$$

$$\bar{C}_{ai} = c_{os} \sum_{bj} E_{aibj}\bar{E}_{bj}. \tag{40}$$

The doubles part of a right eigenvector can be calculated as:

$$E_{aibj} = -\frac{S^{ab}_{ij}\left(\sum_Q \bar{B}^Q_{ai}\hat{B}^Q_{bj}\right)}{\epsilon_a - \epsilon_i + \epsilon_b - \epsilon_j - \omega}, \tag{41}$$

with the three-index intermediates:

$$\bar{B}^p_{pq} = \sum_{\alpha\beta Q} \left(\bar{\Lambda}^p_{\alpha p}\Lambda^h_{\beta q} + \Lambda^p_{\alpha p}\bar{\Lambda}^h_{\beta q}\right)(\alpha\beta|Q)\left[V^{-1/2}\right]_{Qp} \tag{42}$$

built with transformation matrices $\bar{\Lambda}^p = -\mathbf{C}E_1^T$ and $\bar{\Lambda}^h = \mathbf{C}E_1$. The doubles part of a left eigenvector:

$$\bar{E}_{aibj} = -\frac{S^{ab}_{ij}\left(\sum_P B^P_{ai}\bar{\breve{B}}^P_{bj} + \hat{\bar{F}}_{ia}\bar{E}_{bj}\right)}{\epsilon_a - \epsilon_i + \epsilon_b - \epsilon_j + \omega} \tag{43}$$

is formed similar to the doubles part of the ground state Lagrange multipliers in Eq. (17), where $\bar{\breve{B}}^P_{ai}$ depends on the singles part of the left eigenvector $\bar{E}_1$ instead of $\bar{t}_1$. The fourth order scaling algorithm for the calculation of P^A_{ij}, P^A_{ab} and $\bar{C}_{ai}$ is sketched in Fig. 1. During the calculation of P^A_{ij} and P^A_{ab} the frequency ω from the denominators is incorporated in the prefactors:

$$g^z_{ij}(\omega) = \frac{e^{(\epsilon_i+\omega)t_z} - e^{(\epsilon_j+\omega)t_z}}{\epsilon_i - \epsilon_j} = t_z e^{(\epsilon_i+\epsilon_j+2\omega)t_z/2} \frac{\sinh\left[(\epsilon_i - \epsilon_j)t_z/2\right]}{(\epsilon_i - \epsilon_j)t_z/2}, \tag{44}$$

loop over z

  loop over J

    read $\hat{B}^Q_{bj}$, $\bar{B}^Q_{bj}$, B^P_{bj}, $\bar{\breve{B}}^P_{bj}$ for $j \in J$

    $\hat{K}^Q_{bj,z} \leftarrow \hat{B}^Q_{bj} \cdot e^{-t_z(\epsilon_b - \epsilon_j)}$

    $N^{QP}_z \leftarrow \sum_{bj} \hat{K}^Q_{bj,z} B^P_{bj}$, $\quad \breve{N}^{QP}_z \leftarrow \sum_{bj} \hat{K}^Q_{bj,z} \bar{\breve{B}}^P_{bj}$

    $n^Q_z \leftarrow \sum_{bj} \hat{K}^Q_{bj,z} \hat{F}_{jb}$, $\quad \breve{n}^Q_z \leftarrow \sum_{bj} \hat{K}^Q_{bj,z} \bar{E}_{bj}$

    $\bar{K}^Q_{bj,z} \leftarrow \bar{B}^Q_{bj} \cdot e^{-t_z(\epsilon_b - \epsilon_j)}$

    $\bar{N}^{QP}_z \leftarrow \sum_{bj} \bar{K}^Q_{bj,z} B^P_{bj}$, $\quad \bar{\breve{N}}^{QP}_z \leftarrow \sum_{bj} \bar{K}^Q_{bj,z} \bar{\breve{B}}^P_{bj}$

    $\bar{n}^Q_z \leftarrow \sum_{bj} \bar{K}^Q_{bj,z} \hat{F}_{jb}$, $\quad \bar{\breve{n}}^Q_z \leftarrow \sum_{bj} \bar{K}^Q_{bj,z} \bar{E}_{bj}$

  end loop over J

  scale N^{QP}_z, $\bar{N}^{QP}_z$, $\breve{N}^{QP}_z$, $\bar{\breve{N}}^{QP}_z$, n^Q_z, $\breve{n}^Q_z$, $\bar{n}^Q_z$, $\bar{\breve{n}}^Q_z$ with $-c_{os}w_z$

  loop over I

    read $\hat{B}^Q_{ai}$, $\bar{B}^Q_{ai}$, B^P_{ai}, $\bar{\breve{B}}^P_{bi}$ and $\breve{Y}^Q_{ai}$, $\bar{\breve{Y}}^Q_{ai}$ for $i \in I$

    $\breve{Y}^Q_{aiz} \leftarrow \sum_P \left(\breve{N}^{QP}_z B^P_{ai,z} + N^{QP}_z \bar{\breve{B}}^P_{ai,z}\right) + \breve{n}^Q_z \hat{F}_{ia} + n^Q_z \bar{E}_{ai}$

    $\bar{\breve{Y}}^Q_{aiz} \leftarrow \sum_P \left(\bar{\breve{N}}^{QP}_z B^P_{ai,z} + \bar{N}^{QP}_z \bar{\breve{B}}^P_{ai,z}\right) + \bar{\breve{n}}^Q_z \hat{F}_{ia} + \bar{n}^Q_z \bar{E}_{ai}$

    loop over a,b

      $P_{ab} \leftarrow \sum_{Qiz} g^z_{ab}(\omega)\left(\breve{Y}^Q_{aiz}\hat{B}^Q_{bi} + \breve{Y}^Q_{aiz}\bar{B}^Q_{bi}\right) \cdot e^{t_z\epsilon_i}$

    end loop over a,b

    loop over J

      read $\hat{B}^Q_{aj}$, $\bar{B}^Q_{aj}$ for $j \in J$

      loop over a

        $P_{ij} \leftarrow \sum_{Qaz} g^z_{ij}(\omega)\left(\bar{\breve{Y}}^Q_{aiz}\hat{B}^Q_{aj} + \breve{Y}^Q_{aiz}\bar{B}^Q_{aj}\right) \cdot e^{-t_z\epsilon_a}$

      end loop over a

    end loop over J

    $\bar{C}_{ai} \leftarrow \sum_{Qz}\left(\breve{n}^Q_z \bar{B}^Q_{ai} + \bar{\breve{n}}^Q_z \hat{B}^Q_{ai}\right) \cdot e^{-t_z(\epsilon_a - \epsilon_i - \omega)}$

    $\breve{Y}^Q_{ai} \leftarrow \sum_z \breve{Y}^Q_{aiz} \cdot e^{-t_z(\epsilon_a - \epsilon_i - \omega)}$, $\quad \bar{\breve{Y}}^Q_{ai} \leftarrow \sum_z \bar{\breve{Y}}^Q_{aiz} \cdot e^{-t_z(\epsilon_a - \epsilon_i - \omega)}$

    store $\breve{Y}^P_{ai}$, $\bar{\breve{Y}}^P_{ai}$ on file

  end loop over I

end loop over z

Fig. 1. Algorithm for the calculation of the SOS–CC2 one-particle density matrix $D^{F,A}(\bar{E}, E)$.

Author's personal copy

and

$$g^z_{ab}(\omega) = -\frac{e^{-(\epsilon_a-\omega)t_z} - e^{-(\epsilon_b-\omega)t_z}}{\epsilon_a - \epsilon_b} = t_z e^{-(\epsilon_a+\epsilon_b-2\omega)t_z/2}\ \frac{\sinh\left[(\epsilon_a-\epsilon_b)t_z/2\right]}{(\epsilon_a-\epsilon_b)t_z/2}. \quad (45)$$

In the scheme presented in Fig. 1 the Laplace independent intermediates:

$$\breve{Y}^Q_{ai}(\overline{E}) = c_{os}\sum_{bj}\overline{E}_{aibj}\widehat{B}^Q_{bj}, \quad (46)$$

$$\breve{\overline{Y}}^Q_{ai}(\overline{E}) = c_{os}\sum_{bj}\overline{E}_{aibj}\overline{B}^Q_{bj}, \quad (47)$$

are calculated from $\breve{Y}^Q_{aiz}$ and $\breve{\overline{Y}}^Q_{aiz}$ by summation over the quadrature points (compare Eq. (34)). In addition to the scheme in Fig. 1 the intermediates:

$$\overline{Y}^P_{ai}(E) = c_{os}\sum_{bj}E_{aibj}B^P_{bj}, \quad (48)$$

$$\widetilde{Y}^P_{ai}(E) = c_{os}\sum_{bj}E_{aibj}\breve{B}^P_{bj}, \quad (49)$$

are needed to evaluate the two-particle density. They can be obtained as:

$$\overline{Y}^P_{ai}(E) = -c_{os}\sum_{Qz}w_z\left(N^{PQ}_z\overline{B}^Q_{ai} + \overline{N}^{PQ}_z\widehat{B}^Q_{ai}\right)e^{-(\epsilon_a-\epsilon_i)t_z}, \quad (50)$$

$$\widetilde{Y}^P_{ai}(E) = -c_{os}\sum_{Qz}w_z\left(\breve{N}^{PQ}_z\overline{B}^Q_{ai} + \breve{\overline{N}}^{PQ}_z\widehat{B}^Q_{ai}\right)e^{-(\epsilon_a-\epsilon_i)t_z}. \quad (51)$$

For the calculation of transition moments the one-particle density $D^{\eta}_{pq}(E)$ is needed (see Eq. (11)). The doubles contributions to $D^{\eta}_{pq}(E)$ are formed in the same way as the doubles contributions to $D^{A}_{pq}(\overline{E},E)$ in Eqs. (38)–(40), where the left eigenvector $\overline{E}$ is replaced by the ground state lagrange multipliers $\bar{t}^{gs}$. As the doubles part of a left eigenvector is formed similar to the doubles part of the ground state Lagrange multipliers (compare Eqs. (17) and (43)), the algorithm for the calculation of $D^{\eta}_{pq}(E)$ is analogous to the algorithm for $D^{F,A}_{pq}(\overline{E},E)$. Additionally the one-particle densities $D^{\xi}_{pq}(\overline{M})$ and $D^{\xi}_{pq}(\overline{E})$ are needed (see Eqs. (11) and (12)). The doubles part of $\overline{M}$ can be calculated similar to $\bar{t}^{ex}_{aibj}$ in Eq. (36) and $\overline{E}_2$ is analogous to the doubles contribution of $\bar{t}^{gs}$ in Eq. (17), so that these densities can again be evaluated using the same algorithms. For the calculation of transition moments for one-electron operators no two-particle densities are required.

All statements, that were made in this section, also hold for the fourth order scaling algorithm for SOS–ADC(2) with the modification, that the singles parts of the ground state cluster amplitudes t_1 and the Lagrange multipliers $\bar{t}^{gs}_1$ and $\bar{t}^{ex}_1$ are zero. Thereby the similarity-transformed three-index-intermediates $\widehat{B}^P_{ai}$ become identical to the unmodified intermediates B^P_{ai} and the intermediates $\breve{B}^P_{ai}$ in Eqs. (18) and (36), which depend on the singles part of the Lagrange multipliers, are zero. The intermediate $\breve{B}^P_{ai}$ in Eq. (43) does not change, as it depends on the singles part of the left eigenvector $\overline{E}_1$. The relation between the algorithms for CC2 and ADC(2) in general is described in Ref. [17].

4. Results

4.1. Laplace error

A measure for the accuracy of the numerical Laplace transformation introduced in Eq. (22) is the integral over the squared error:

$$F^{\mathrm{Lap}}(t_z) = \int_{\epsilon_{\min}}^{\epsilon_{\max}}\left(\frac{1}{\epsilon_{aibj}} - \sum_z^n w_z e^{-\epsilon_{aibj}t_z}\right)^2 d\epsilon_{aibj}. \quad (52)$$

In our previous publication [10] we determined the Laplace error for ground state and vertical excitation energies. In the present work we consider the Laplace error of adiabatic electronic excitation energies and structure parameters in electronically excited states. Therefore we had a look at the test set from Ref. [2], which was used to demonstrate the accuracy of the RI approximation for excited state gradients with CC2. We chose those molecules from the test set, which were not yet investigated with SOS–CC2 in Ref. [7] and carried out SOS–CC2 calculations with different convergence criteria for F^{Lap} using the aug-cc-pVQZ [22–24] basis set and employing the frozen-core approximation. For Mg_2 we used the aug-cc-pCVQZ [25] basis set instead and kept only the electrons in the 1s orbitals frozen.

The error in adiabatic excitation energies introduced by the numerical Laplace transformation, denoted in the following as Laplace error ΔE^{Lap}, is defined as:

$$\Delta E^{\mathrm{Lap}} = E_{\mathrm{SOS}} - E^{\mathrm{Lap}}_{\mathrm{SOS}}, \quad (53)$$

where $E^{\mathrm{Lap}}_{\mathrm{SOS}}$ is the adiabatic excitation energy calculated using the fourth order scaling Laplace-transformed algorithm and E_{SOS} is the SOS excitation energy calculated with the conventional fifth order scaling algorithm. The Laplace error in bond distances and angles in excited states is determined in the same way.

The results for the Laplace error in adiabatic electronic excitation energies are collected in Table 1. In Ref. [10] it was found that the Laplace error in vertical excitation energies correlates with the Laplace error function from Eq. (52) by the relation:

Table 1
0–0 transition energies (eV) and the Laplace errors (meV) for SOS–CC2 with different convergence criteria for the Laplace error function F^{Lap} (a.u). For Mg_2 the adiabatic excitation energy is given.

Molecule	State	T_e				Laplace error for F^{Lap} lower than			
		Exp.	CC2[a]	SOS–CC2	SOS–ADC(2)	10^{-8}	10^{-6}	10^{-4}	10^{-2}
Mg_2[b]	$1\,^1\Sigma^+_u$	3.23	3.28	3.29	3.27	0.19	1.22	7.41	−34.46
C_3[c]	$1\,^1\Pi_u$	3.06	3.08	3.50	3.58	0.85	3.43	9.97	76.28
C_2H_2c	$1\,^1A_u$	5.23	5.33	5.36	5.32	0.02	0.00	3.46	10.93
CH_2O[d]	$1\,^1A''$	3.49	3.52	3.71	3.53	0.11	0.37	5.38	18.01
	$1\,^3A''$	3.12	3.05	3.34	3.22	0.04	0.12	2.52	−14.13
CH_2Se	$1\,^1A_2$	2.03	2.15	2.23	2.11	0.10	0.51	4.13	18.42
	$1\,^3A''$	1.80	1.79	1.98	1.89	0.02	0.35	1.50	−2.78
Trans-$(CHO)_2$c	$1\,^1A_u$	2.72	2.70	3.03	2.95	0.04	0.16	2.18	7.85
HC_2CHOc	$1\,^1A''$	3.24	3.17	3.51	3.28	0.16	0.54	5.30	60.53

[a] The results are identical to those reported in Ref. [2].
[b] Exp. value from Ref. [28].
[c] Exp. values from Ref. [29].
[d] Exp. values from Ref. [30].

Author's personal copy

Table 2
Excited state structure parameters and the Laplace error for SOS–CC2 (bond lengths in pm and angles in degrees) with different convergence criteria for the Laplace error function F^{Lap}. For Mg_2 the experimental r_e-value is quoted which is corrected for vibrational effects.

Molecule	State	Parameter	Exp.	CC2[a]	SOS–CC2	SOS–ADC(2)	Laplace error for F^{Lap} lower than			
							10^{-8}	10^{-6}	10^{-4}	10^{-2}
Mg_2[b]	$1\,^1\Sigma_u^+$	r_e	308.2	310.9	314.7	314.2	−0.011	−0.047	−0.162	−0.486
C_3[c]	$1\,^1\Pi_u$	d(CC)	130.5	132.2	131.4	130.4	0.006	0.036	0.083	0.313
C_2H_2[d]	$1\,^1A_u$	d(CC)	137.5	138.1	137.3	136.9	0.000	0.000	−0.006	−0.406
		d(CH)	110.0	109.1	109.2	109.1	0.000	0.000	−0.003	−0.308
		∠(HCC)	122.5	122.0	122.3	122.4	0.000	0.000	0.008	0.350
CH_2O[e]	$1\,^1A''$	d(CH)	109.8	108.7	109.0	108.7	0.000	−0.001	−0.017	−0.434
		d(CO)	132.3	135.5	134.2	135.9	0.004	0.016	0.143	0.491
		∠(HCH)	118.4	121.5	120.0	121.6	0.000	0.002	0.037	0.045
		ϕ	34.0	25.9	28.1	22.2	0.005	0.016	0.111	1.301
	$1\,^3A''$	d(CH)	108.4	109.2	109.4	109.2	0.000	−0.001	−0.012	−0.402
		d(CO)	130.7	133.6	132.4	133.1	0.002	0.006	0.061	−0.049
		∠(HCH)	117.9	117.8	116.7	118.1	0.000	0.001	0.028	0.060
		ϕ	41.1	38.2	38.6	35.2	0.001	0.003	0.019	0.081
CH_2S[e]	$1\,^1A_2$	d(CH)	107.7	108.3	108.3	108.3	0.000	0.000	−0.005	−0.295
		d(CS)	168.2	170.6	170.4	171.6	0.004	0.014	0.103	0.352
		∠(HCH)	120.7	121.1	120.4	120.4	0.001	0.003	0.024	0.133
	$1\,^3A''$	d(CH)	108.2	108.2	108.2	108.2	0.000	−0.001	0.001	−0.266
		d(CS)	168.3	168.8	168.6	169.0	0.002	0.015	0.046	−0.063
		∠(HCH)	119.3	120.9	120.3	120.6	−0.001	−0.002	−0.016	−0.049
		ϕ	11.9	11.9	9.9	3.4	0.012	0.081	0.318	0.617
Trans-$(CHO)_2$[f]	$1\,^1A_u$	d(CC)	146.0	147.9	148.9	148.7	−0.001	−0.006	−0.084	−1.397
		d(CH)	112.0	109.5	109.4	109.4	0.000	0.000	−0.009	−0.440
		d(CO)	125.0	125.4	124.7	124.5	0.001	0.003	0.041	0.057
		∠(HCC)	114.0	114.5	114.5	114.9	0.001	0.002	0.044	0.497
		∠(OCC)	124.0	123.9	123.5	123.3	0.000	0.000	−0.007	−0.065
HC_2CHO[c]	$1\,^1A''$	$d(C_1C_2)$	123.8	123.6	122.5	122.0	0.001	0.003	0.024	0.134
		$d(C_3H)$	109.1	108.5	108.5	108.4	0.000	−0.001	−0.011	−0.435
		$d(C_3O)$	132.5	140.6	137.4	139.8	0.004	0.015	0.182	0.583

[a] The results are identical to those reported in Ref. [2].
[b] Exp. data from Ref. [28].
[c] Exp. data from Ref. [29].
[d] Exp. data from Ref. [31].
[e] Exp. data from Ref. [30].
[f] Exp. data from Ref. [32].

$$\left|\Delta E^{Lap}\right| \leqslant \sqrt{F^{Lap}}. \tag{54}$$

That means enforcing $\sqrt{F^{Lap}} \leqslant 10^{-4}$ results in an absolute Laplace error of less than 0.1 mH or 2.7 meV in the energy. As can be seen from Table 1 the Laplace error for adiabatic electronic excitation energies is about one order of magnitude lower than this for all cases. A convergence criterion of $\sqrt{F^{Lap}} \leqslant 10^{-3}$ should result in an error of less than 1 mH or 27 meV. Again the Laplace error is about one order of magnitude lower than this also in the worst case ($1\,^1\Pi_u$ state of C_3). $\sqrt{F^{Lap}} \leqslant 10^{-2}$ should result in an energy error of less than 270 meV and $\sqrt{F^{Lap}} \leqslant 10^{-1}$ in an error of less than 2700 meV. It can clearly be seen that such Laplace errors are not reached. The errors for the adiabatic excitation energies are typically about one order of magnitude smaller than for vertical excitation energies. This is due to a systematic error cancellation in the ground and excited state. We note that this error cancellation takes only place when the same number of Laplace grid points is used for the ground and the excited state calculation. If a different number of points is used, the Laplace error increases significantly.

In Table 2 the Laplace errors for structure parameters of electronically excited states are listed. With a convergence criterion of $\sqrt{F^{Lap}} \leqslant 10^{-4}$ the largest absolute error in a bond length is 0.011 pm for Mg_2. For angles the maximum error is 0.012° for the dihedral angle of CH_2S. Enforcing $\sqrt{F^{Lap}} \leqslant 10^{-3}$ results in a maximum absolute error of 0.05 pm for Mg_2 and 0.08° for the dihedral angle of CH_2S. Even with very loose convergence criteria of $\sqrt{F^{Lap}} \leqslant 10^{-2}$ and $\sqrt{F^{Lap}} \leqslant 10^{-1}$ the Laplace errors in bond angles remain below 0.5° and 1° and the maximum errors observed for bond lengths are still below 0.2 pm and 0.6 pm respectively. Altogether we find that the Laplace errors of structure parameters in excited states are very small and already with a small number of grid points insignificant compared to the inherent accuracy of CC2 and ADC(2).

The Laplace error of transition moments has also been investigated. Since for most of the states in the test set for structures the oscillator strengths are zero or very small, we studied the Laplace error in oscillator strengths for some selected molecules from the test set for vertical excitation energies reported in Ref. [10]. For these molecules SOS–CC2 calculations with different convergence criteria for F^{Lap} were carried out. For these calculations the aug-cc-pVTZ [22–24] basis set and the frozen-core approximation were employed. The results are listed in Table 3. With $\sqrt{F^{Lap}} \leqslant 10^{-3}$ and $\sqrt{F^{Lap}} \leqslant 10^{-2}$ the Laplace errors in oscillator strengths are completely negligible. The highest error occurs for the $3\,^1A_1$ state of pyrimidine and is with both convergence criteria still smaller than 2% of the oscillator strength. For $\sqrt{F^{Lap}} \leqslant 10^{-1}$ the Laplace error is at most 7% of the oscillator strength for the $2\,^1A'$ state of formamide. Even with this high value of the Laplace error function the errors in oscillator strengths are very small.

To get $\sqrt{F^{Lap}} \leqslant 10^{-1}$ three grid points were needed for Mg_2. For all other molecules considered here only two grid points were sufficient. For Mg_2 the aug-cc-pCVQZ basis set was used and therefore the range of orbital energies is larger than for the other molecules, so

Author's personal copy

Table 3
Oscillator strengths (length gauge) and the Laplace errors for SOS–CC2 with different convergence criteria for the Laplace error function F^{Lap}.

Molecule	State	CC2	SOS–CC2	SOS–ADC(2)	Laplace error (for F^{Lap} lower than)		
					10^{-6}	10^{-4}	10^{-2}
Naphthalene	$1\,^1B_{3u}$	0.0000	0.0002	0.0001	0.0000	0.0000	0.0000
	$1\,^1B_{2u}$	0.0777	0.0587	0.0731	0.0000	0.0000	−0.0007
	$2\,^1B_{3u}$	1.4238	1.5119	1.8228	0.0001	0.0004	0.0019
	$2\,^1B_{2u}$	0.2532	0.3105	0.3906	−0.0001	−0.0005	−0.0038
Furan	$1\,^1B_2$	0.1838	0.1700	0.2067	0.0000	0.0002	0.0016
	$2\,^1A_1$	0.0003	0.0009	0.0015	0.0000	0.0000	−0.0003
	$3\,^1A_1$	0.3579	0.4164	0.3924	0.0004	0.0018	0.0139
Pyrimidine	$1\,^1B_1$	0.0054	0.0060	0.0059	0.0000	0.0000	0.0001
	$1\,^1B_2$	0.0292	0.0246	0.0284	0.0000	0.0001	0.0001
	$2\,^1A_1$	0.0860	0.0282	0.0318	0.0000	−0.0001	−0.0020
	$3\,^1A_1$	0.4100	0.3173	0.1677	0.0014	0.0053	−0.0102
	$2\,^1B_2$	0.5151	0.5170	0.5783	0.0003	0.0013	0.0032
Formaldehyde	$1\,^1B_1$	0.0009	0.0012	0.0014	0.0000	0.0000	0.0000
	$2\,^1A_1$	0.0826	0.1476	0.1782	0.0001	0.0014	0.0054
Acetone	$1\,^1B_1$	0.0005	0.0000	0.0000	0.0000	0.0000	0.0000
p-Benzoquinone	$1\,^1B_{1u}$	0.5305	0.6180	0.6808	0.0000	0.0005	0.0040
Formamide	$1\,^1A''$	0.0004	0.0004	0.0004	0.0000	0.0000	0.0000
	$2\,^1A'$	0.3180	0.2417	0.1705	0.0006	0.0033	0.0160

that more grid points are needed. Their number could be reduced by deleting very high lying virtual orbitals, which we did not exploit in this study. Setting the criterion for the Laplace error function to $\sqrt{F^{Lap}} \leqslant 10^{-2}$ five grid points were employed for Mg_2 and three or four points for all other molecules. Enforcing $\sqrt{F^{Lap}} \leqslant 10^{-3}$ results in five to six grid points (seven for Mg_2) and to get $\sqrt{F^{Lap}} \leqslant 10^{-4}$ seven quadrature points are needed (nine for Mg_2). This means, that already with a low number of grid points one can obtain a satisfying accuracy of the numerical Laplace transformation.

4.2. Accuracy of SOS–CC2 and SOS–ADC(2)

The accuracy of SOS–CC2 for adiabatic electronic excitation energies, structure parameters in the ground and excited state and harmonic vibrational frequencies has already been investigated in Ref. [7]. In the present work we studied the accuracy of SOS–ADC(2) for adiabatic electronic excitation energies, excited state structure parameters, harmonic vibrational frequencies as well as dipole moments and transition strengths and compared with SOS–CC2 and unscaled CC2 results. For this we used the test sets described in Section 4.1. To investigate harmonic vibrational frequencies and dipole moments the same test set was used as for adiabatic electronic excitation energies and excited state structure parameters, whereas for transition strengths some states from the test set for vertical excitation energies from Ref. [10] were examined.

The structures of the molecules were optimized in the ground and excited state with CC2, SOS–CC2 and SOS–ADC(2) using the TURBOMOLE program package [11]. Harmonic vibrational frequencies were obtained by numerical differentiation of the analytical gradients and dipole moments were calculated for ground and excited states. For all calculations the aug-cc-pVQZ [22–24] basis set and the frozen-core approximation were employed.

We note that we did not allow unphysical symmetry breaking during the geometry optimizations. CC2 and SOS–ADC(2) do not provide equilibrium geometries for the $1\,^1\Pi_u$ state of C_3 under this condition, as can be seen from an imaginary frequency in the vibrational spectrum. SOS–ADC(2) reveals in addition an imaginary frequency for the $1\,^1A_u$ state of C_2H_2.

0–0 transition energies are listed in Table 1. For Mg_2 the adiabatic excitation energy is given since for this an experimental reference value exists. As already pointed out in Ref. [7] adiabatic excitation energies have a systematic blue-shift with SOS–CC2. For all molecules except C_3 SOS–ADC(2) gives results which are less blue shifted than with SOS–CC2. The difference is especially emphasized for the aldehydes and thioaldehydes, which represent four of the seven considered molecules. For vertical excitation energies of molecules with a double bonded oxygen, like aldehydes and amides, SOS–ADC(2) is also significantly less blue shifted than SOS–CC2. [10] For all other vertical excitation energies investigated in Ref. [10] the results with SOS–ADC(2) differ only slightly from the SOS–CC2 results. Unscaled ADC(2) provides already too low adiabatic excitation energies for the $1\,^1A''$ and $1\,^3A''$ state of CH_2O, whereas on average adiabatic excitations energies with ADC(2) are blue shifted with respect to CC2. [17] Therefore the SOS–ADC(2) method benefits from a good error cancellation in the case of aldehydes.

SOS–CC2 and SOS–ADC(2) have relatively large errors of 0.44 eV and 0.52 eV for the $1\,^1\Pi_u$ state of C_3. As already unscaled CC2 does not provide an equilibrium geometry of the $1\,^1\Pi_u$ state of C_3 with the correct symmetry, the description of this state seems to be difficult with second order methods.

Excited state structures parameters are listed in Table 2. CC2 overestimates bond lengths, as already pointed out in Ref. [2]. This error is reduced by SOS–CC2, which is in agreement with the results from Ref. [7]. This effect is especially pronounced for the C—O bond of aldehydes in the $n\pi^*$ excited states. With CC2 the C—O bond is about 3 pm to long for the $1\,^1A''$ and $1\,^3A''$ states of formaldehyde. The C—O bond for the $1\,^1A''$ state of HC_2CHO is approximately 8 pm to long. With SOS–CC2 the bond lengths of the $1\,^1A''$ and $1\,^3A''$ states of formaldehyde are merely about 2 pm to long and the C—O bond of HC_2CHO is about 5 pm to long. The same trend is seen for the C—S bond in the excited states of thioformaldehyde. The bond lengths are too long with CC2 and the error is again reduced with SOS–CC2, although the effect is not as pronounced as for the C—O bonds.

No such systematic improvement upon CC2 is seen for SOS–ADC(2). SOS–ADC(2) provides even shorter bond lengths than SOS–CC2 for most of the C—H and C—C bonds, which can lead to an over-correction e.g. for the C—C bond in the $1\,^1A_u$ state of C_2H_2 and the C_1—C_2 bond of HC_2CHO. For the C—O and C—S bonds of formaldehyde, thioformaldehyde and HC_2CHO SOS–ADC(2) yields longer bond lengths than SOS–CC2, partially even longer than with unscaled CC2.

For all C—H, C—C, C—O and C—S bonds the spin scaled methods deviate less than 2 pm from the CC2 reference results. For the bond

Author's personal copy

lengths of the test set the deviation is only higher in the case of Mg_2, where the spin scaling has an exceptional large effect because of the weak bond.

We note that only SOS–CC2 provides qualitatively correct equilibrium structures for all molecules and states in the test set. Unscaled CC2 fails for the equilibrium structure of C_3, where it provides an imaginary frequency when the correct symmetry is enforced. SOS–ADC(2) predicts as well an imaginary frequency for C_3. Additionally it yields an imaginary frequency for C_2H_2 when a symmetry constraint is applied.

Harmonic vibrational frequencies are listed in Table 4. Since the experimental reference data are not corrected for anharmonicities, the calculated frequencies are expected to be slightly higher than the experimental ones. For the $\nu_2(\sigma_u)$ mode of C_3 in the $1\,^1\Pi_u$ state CC2 and SOS–ADC(2) give imaginary frequencies, whereas this mode is reproduced well with SOS–CC2. We note that the present CC2 results for the modes of C_3 are different from the values reported in Ref. [2] for the same basis set, which do not fit to the frequencies reported in the same reference for smaller basis sets and are probably incorrect.

For the C—O stretch modes in the $1\,^1A''$ state of CH_2O ($\nu_3(a')$) and in the $1\,^1A''$ state of HC_2CHO ($\nu_6(a')$) SOS–CC2 performs significantly better than CC2 and SOS–ADC(2). This is also the case for the C—S stretch modes of CH_2S ($\nu_3(a_1)$ in the $1\,^1A_2$ state and $\nu_3(a')$ in the $1\,^3A''$ state), but the differences between the methods are not as pronounced as for the C—O stretch modes. This effect is related to the smaller error of SOS–CC2 for the bond lengths of the C—O and C—S bonds. For most of the other frequencies the results with unscaled CC2 and the spin scaled methods do not differ much.

Dipole moments for ground and excited states of CH_2O and CH_2S are listed in Table 5. The dipole moments obtained with CC2 and SOS–CC2 deviate by at most 0.12 D in the unrelaxed formulation. In the relaxed formulation the differences are even smaller. The SOS–ADC(2) dipole moments differ by up to 0.24 D from the CC2 results.

Oscillator strengths for some selected molecules from the test set reported in Ref. [10] are listed in Table 3. The oscillator strengths of the spin scaled methods are in all cases of the same order of magnitude as with unscaled CC2. For the $2\,^1A_1$ and $3\,^1A_1$ states of pyrimidine, the $2\,^1A_1$ state of formaldehyde and the $2\,^1A'$ state

Table 4
Harmonic vibrational frequencies (cm^{-1}). For Mg_2 the experiment al ω_e-value is quoted which is corrected for anharmonicities.

Molecule	State	Mode	Exp.	CC2[a]	SOS–CC2	SOS–ADC(2)
Mg_2[b],	$1\,^1\Sigma_u^+$	ω_e	190.6	181.2	177.4	179.4
C_3[c,d]	$1\,^1\Pi_u$	$\nu_1(\sigma_g)$	1085.9	1069.4	1118.5	1172.6
		$\nu_2(\sigma_u)$	541.7	i843.0	580.3	i851.0
		$\nu_3(\pi_u)$	307.9	260.2	246.7	238.3
C_2H_2[c]	$1\,^1A_u$	$\nu_2(a_g)$	1385.0	1367.5	1405.9	1435.4
		$\nu_3(a_g)$	1047.6	1085.3	1102.5	1105.0
CH_2O[e]	$1\,^1A''$	$\nu_1(a')$	2846.0	3062.0	3043.4	3072.6
		$\nu_2(a')$	1293.1	1320.3	1347.8	1367.5
		$\nu_3(a')$	1183.0	1014.0	1093.6	1002.2
		$\nu_5(a'')$	2968.3	3198.9	3163.4	3200.0
		$\nu_6(a'')$	904.0	870.4	905.9	905.9
	$1\,^3A''$	$\nu_2(a')$	1283.0	1297.4	1324.4	1344.2
CH_2S[e]	$1\,^1A_2$	$\nu_1(a_1)$	3034.0	3125.8	3121.8	3121.4
		$\nu_2(a_1)$	1320.0	1342.3	1374.5	1377.9
		$\nu_3(a_1)$	859.0	798.1	812.4	796.7
		$\nu_4(b_1)$	3081.3	3251.7	3239.6	3241.1
		$\nu_5(b_1)$	799.0	765.1	791.2	771.8
	$1\,^3A''$	$\nu_2(a')$	1320.0	1335.8	1368.1	1372.8
		$\nu_3(a')$	859.0	845.5	862.3	841.8
Trans-$(CHO)_2$[f]	$1\,^1A_u$	$\nu_1(a_g)$	2809.0	3049.9	3054.8	3068.9
		$\nu_2(a_g)$	1391.4	1368.3	1418.9	1443.5
		$\nu_3(a_g)$	1195.2	1230.6	1246.4	1264.5
		$\nu_4(a_g)$	952.4	993.6	985.9	1007.6
		$\nu_5(a_g)$	508.9	493.8	500.4	508.2
		$\nu_6(a_u)$	720.0	753.5	754.6	757.4
		$\nu_7(a_u)$	233.2	218.8	221.6	220.8
		$\nu_8(b_g)$	735.1	763.3	753.7	769.1
		$\nu_{10}(b_u)$	1280.8	1247.1	1242.7	1235.7
		$\nu_{11}(b_u)$	1172.0	1175.9	1203.5	1092.7
		$\nu_{12}(b_u)$	379.3	369.5	384.0	385.2
HC_2CHO[c]	$1\,^1A''$	$\nu_2(a')$	2952.5	3168.7	3159.4	3176.0
		$\nu_3(a')$	1945.8	1896.7	1996.8	2044.8
		$\nu_4(a')$	1304.0	1217.7	1269.3	1262.8
		$\nu_5(a')$	1119.5	1072.8	1067.8	1063.1
		$\nu_6(a')$	951.6	777.1	903.0	832.3
		$\nu_7(a')$	650.0	639.4	665.5	695.2
		$\nu_8(a')$	506.9	470.7	486.5	494.6
		$\nu_9(a')$	189.4	170.2	176.4	179.1
		$\nu_{10}(a'')$	506.9	549.3	476.9	505.1
		$\nu_{11}(a'')$	389.7	408.2	420.8	453.8
		$\nu_{12}(a'')$	345.9	325.8	336.0	340.3

[a] With the exception of the modes for C_3 the results are within the numerical accuracy identical to those reported in Ref. [2].
[b] Exp. data from Ref. [28].
[c] Exp. data from Ref. [29].
[d] Exp. data for mode $\nu_2(\sigma_u)$ from Ref. [33].
[e] Exp. data from Ref. [30].
[f] Exp. data from Ref. [34].

Author's personal copy

Table 5
Dipole moments (D) of CC2 and SOS–CC2 in the unrelaxed and relaxed formulation. For SOS–ADC(2) only relaxed dipole moments are given. Exp. values are taken from Ref. [30].

Molecule	State	Exp.	CC2[a]		SOS–CC2		SOS–ADC(2)
CH_2O	$X\ ^1A_1$	2.33	2.27[b]	2.38	2.33	2.42	2.42[c]
	$1\ ^1A''$	1.56	1.10	1.73	1.22	1.73	1.97
	$1\ ^3A''$	1.29	1.08	1.46	1.16	1.47	1.62
CH_2S	$X\ ^1A_1$	1.65	1.66	1.72	1.69	1.73	1.67[c]
	$1\ ^1A_2$	0.79	0.38	0.96	0.45	0.94	1.16
	$1\ ^3A''$	0.57	0.24	0.55	0.25	0.54	0.66

[a] With the exception of the unrelaxed value for the $X\ ^1A_1$ state of CH_2O the results are identical to those reported in Ref. [2].
[b] Note that the unrelaxed CC2/aug-cc-pVTZ value reported in Ref. [2] is incorrect.
[c] For the ground state results from SOS-MP2 are given.

of formamide the character of the excitations with SOS–CC2 and SOS–ADC(2) differ from the character obtained with CC2. Accordingly the oscillator strengths of the spin scaled methods deviate from the CC2 results by up to a factor of three. For all other states with a valuable oscillator strength SOS–CC2 deviates at most by a factor of 1.3 and SOS–ADC(2) by a factor of 1.5 from the CC2 results.

4.3. Timings

The time-determining steps of the Laplace-transformed SOS–CC2 algorithm are the formation of the N and Y intermediates and the calculation of the one-particle density contributions P_{ij} and P_{ab}. The formation of N and Y scale with $N_x^2 N_o N_v N_L$ (see e.g. Eqs. (26) and (27)), where N_x is the number of auxiliary functions for the RI approximation, N_o is the number of occupied and N_v the number of virtual orbitals and N_L the number of grid points for the numerical quadrature, which is independent of the system size. The operation count for P_{ij} scales with $N_x N_o^2 N_v N_L$ (see Eq. (25)) and that of P_{ab} with $N_x N_o N_v^2 N_L$ (see Eq. (31)). The time-determining steps of the conventional algorithm are the formation of the doubles contributions to the ground state cluster amplitudes t, the Lagrange multipliers $\bar{t}$ and the left and right eigenvectors E and $\bar{E}$ as well as their contraction to Y intermediates. These steps scale with $N_x N_o^2 N_v^2$, where for the four-index quantities the symmetry $t_{ab}^{ij} = t_{ba}^{ji}$ can be exploited so that they only have to be computed for $i \geqslant j$. The calculation of P_{ij} scales with $N_o^3 N_v^2$ and that of P_{ab} with $N_o^2 N_v^3$.

For the ground state density $D_{pq}^{F,\xi}(\bar{t}^{gs})$ with the Laplace-transformed algorithm two N intermediates have to be calculated, $\breve{Y}$ is formed from two contractions and $\widetilde{Y}$ from one contraction of N intermediates (see Eqs. (26) and (35)). To calculate P_{ij} and P_{ab} one additional contraction has to be done for each of them (compare Eqs. (25) and (31)). With the conventional algorithm the ground state cluster amplitudes t and the Lagrange multipliers $\bar{t}^{gs}$ are calculated and contracted to $\breve{Y}$ and $\widetilde{Y}$. If we assume that $N_x \approx 3N_v$, as it is the case for most basis sets, the ratio between the operation counts of the fourth and the fifth order scaling algorithms is roughly $\frac{96}{23}\frac{N_L}{N_o}$ for a ground state density calculation. The higher the prefactor of $\frac{N_L}{N_o}$ is, the smaller are the savings in computational time of the fourth order scaling algorithm. That means that the speed-up for the ground state density is only slightly smaller than for the determination of the cluster amplitudes with a ratio of $4\frac{N_L}{N_o}$, but still higher than for the solution of the eigenvalue problem with a ratio of $\frac{24}{5}\frac{N_L}{N_o}$ [10,26].

For the excited state density $D^{F,A}(\bar{E},E)$ with the Laplace-transformed algorithm four N intermediates are calculated. Two of these are contracted to $\breve{Y}$ and the other two to $\widetilde{Y}$ (compare Fig. 1). Four additional contractions are needed to calculate $\overline{Y}$ and $\widetilde{Y}$ (see Eqs. (50) and (51)). To get P_{ij} and P_{ab} for each of them two contractions are carried out (compare Fig. 1). With the conventional algorithm the doubles contributions to the left and right eigenvectors are formed and contracted to the four Y intermediates. If we again assume $N_x \approx 3N_v$, the ratio between the fourth and the fifth order scaling algorithms is $6\frac{N_L}{N_o}$ for the calculation of $D^{F,A}(\bar{E},E)$. If we compare to the theoretically derived ratio for $D_{pq}^{F,\xi}(\bar{t}^{gs})$ the prefactor of $\frac{N_L}{N_o}$ is higher for the A-density. This means that the speed-up of the fourth order scaling algorithm for $D^{F,A}(\bar{E},E)$ is expected to be smaller than for $D_{pq}^{F,\xi}(\bar{t}^{gs})$.

The computational savings of the fourth order scaling algorithm with increasing system size are shown for a series of glycine polypeptides. The chain length is varied between two and nine glycines. For these test systems ground and excited state gradients were calculated with the TZVP basis set and eight Laplace quadrature points, which provide a high accuracy of the Laplace error function of $F^{\mathrm{Lap}} < 2.5 \times 10^{-8}$ for all chain lengths. In Figs. 2 and 3 the computational timings for the calculation of the ground state density $D_{pq}^{F,\xi}(\bar{t}^{gs})$ and the excited state density $D^{F,A}(\bar{E},E)$ are plotted. The results are fitted to power functions of the chain length N_{gly}:

$$f(N_{\mathrm{gly}}) = \alpha N_{\mathrm{gly}}^5, \tag{55}$$

$$g(N_{\mathrm{gly}}) = \beta N_{\mathrm{gly}}^4. \tag{56}$$

As expected from the estimates for the operation count, the savings with the fourth order scaling algorithm for $D_{pq}^{F,\xi}(\bar{t}^{gs})$ are larger than for $D^{F,A}(\bar{E},E)$. In Fig. 2 one can see that for the ground state density the break-even point is reached with about four glycine units. For $D^{F,A}(\bar{E},E)$ the cross-over occurs somewhat later between five and six glycines (compare Fig. 3). For $D_{pq}^{F,\xi}(\bar{t}^{gs})$ the ratio between the prefactors $\frac{\beta}{\alpha} \approx 4$ is close to the theoretical value of $\frac{96}{23}\frac{N_L}{N_o}$ (with $N_L = 8$ and $\frac{N_o}{N_{\mathrm{gly}}} = 11$). Also for $D^{F,A}(\bar{E},E)$ the ratio $\frac{\beta}{\alpha} \approx 5.9$ fits to the estimate of $6 \cdot \frac{8}{11}$. For the density $D_{pq}^{F,\xi}(\bar{t}^{ex})$ the benefit of the Laplace algorithm is similar to that of $D_{pq}^{F,\xi}(\bar{t}^{gs})$ with a $\frac{\beta}{\alpha}$ ratio of 4.6.

4.4. Applications

To demonstrate the applicability of the Laplace-transformed SOS–CC2 method to gradient and property calculations of large systems, two applications are presented. First we calculated SOS–CC2 gradients of the ground and first excited state as well as transition moments for the chlorophyll molecule. The chlorophyll molecule has 137 atoms and, using the TZVP basis set and the frozen-core approximation for occupied orbitals, 176 valence occupied and 1421 virtual orbitals and 4455 auxiliary basis functions for the RI approximation. We used seven Laplace grid points, which leads to a tight value of the Laplace error function of 6.4×10^{-8}

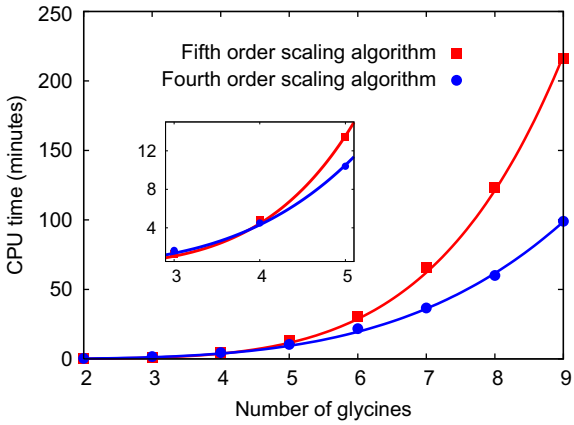


Fig. 2. Timings for SOS–CC2 calculations of the ground state density $D_{pq}^{F,\xi}(\bar{t}^{gs})$ tested at a glycine chain: CPU time (minutes) versus the number of glycines N_{gly}.

Author's personal copy

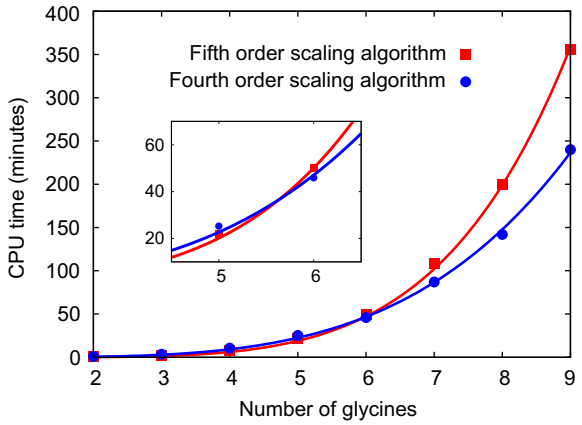


Fig. 3. Timings for SOS–CC2 calculations of the excited state density $D^{F,A}(\bar{E},E)$ tested at a glycine chain: CPU time (minutes) versus the number of glycines N_{gly}.

In the following we will give wall times for the time-determining steps of a calculation on seven processors and estimate the speed-up of the fourth order scaling algorithm compared to the conventional one.

The wall time for the calculation of the ground state density $D^{F,\xi}_{pq}(\bar{t}^{gs})$ was 3 h and 50 min. We estimated a speed-up of a factor of six for the calculation of $D^{F,\xi}_{pq}(\bar{t}^{gs})$ compared to the conventional algorithm. The calculation of the density $D^{F,\xi}_{pq}(\bar{t}^{ex})$ for the excited state gradient was 4 h and 4 min. The calculation takes slightly longer than for $D^{F,\xi}_{pq}(\bar{t}^{gs})$ since one additional Y intermediate has to be calculated. For $D^{F,\xi}_{pq}(\bar{t}^{ex})$ the speed-up of the Laplace-transformed algorithm is estimated to be a factor of 4.9. The calculation of the excited state density $D^{F,A}(\bar{E},E)$ takes 9 h and 17 min under the same conditions. For this density the speed-up is about a factor of 4.2. These speed-ups are already obtained with an accurate grid for the Laplace integration. If the high-lying virtual anti-core orbitals are deleted, seven Laplace grid points provide already a very tight convergence of $F^{\mathrm{Lap}} = 3.6 \times 10^{-10}$. As shown in Section 4.1, much looser convergence criteria of $F^{\mathrm{Lap}} \leqslant 10^{-6}$ or even $F^{\mathrm{Lap}} \leqslant 10^{-4}$ will be sufficient in most cases. For chlorophyll in the TZVP basis these criteria are fulfilled with five and four grid points respectively, if the occupied core and virtual anti-core orbitals are excluded from the correlation treatment. This considerably enhances the speed-up.

For the previously discussed densities also contributions to the corresponding two-particle densities $\hat{d}^{nsep}_{pqrs}$ are needed. The time-determining steps for their construction have been included in the considered computational times. For the densities $D^{\xi}_{pq}(\bar{M}), D^{\xi}_{pq}(\bar{E})$ and $D^{\eta}_{pq}(E)$, which are needed for transition moments (see Eqs. (11) and (12)), only one-particle contributions are calculated. During the calculation of one-particle densities some Y intermediates, that are needed to form the corresponding two particle densities, are obtained as byproducts with negligible additional costs when the fourth order scaling algorithm is applied. In the framework of the fifth order scaling algorithm the Y intermediates for the two-particle densities require additional matrix multiplications with $N_o^2 N_v^2 N_x$ costs. Therefore the benefit of the fourth order scaling algorithm is high for the two-particle densities and somewhat smaller if only one-particle contributions are required. For chlorophyll the calculation of $D^{\xi}_{pq}(\bar{M})$ as well as $D^{\xi}_{pq}(\bar{E})$ requires about three hours on seven processors. The fourth order scaling algorithm gives a speed-up of a factor of 3.5 for these densities. The calculation of $D^{\eta}_{pq}(E)$ takes six hours and the conventional algorithm should take 2.3 times longer. Again, these speed-ups are obtained already with seven grid points for the Laplace integration. If also the virtual anti-core orbitals are deleted and the convergence criterion is relaxed to $F^{\mathrm{Lap}} \leqslant 10^{-6}$ the speed-up increases by a factor of 1.4 and with $F^{\mathrm{Lap}} \leqslant 10^{-4}$ even by a factor of 1.75.

For excited state densities the Laplace SOS–CC2 algorithm still gives a smaller speed-up than for the solution of the eigenvalue problem, where it is faster by a factor of five for the chlorophyll molecule (see Ref. [10] for a detailed discussion). However, for gradient or property calculations most of the computational time is spent on the iterative solution of the ground state cluster equations, the left and right eigenvalue problem and the response equations for the Lagrangian multipliers. For the calculation of a gradient for one excited state of chlorophyll the solution of the linear equation systems require about 1 day and 12 h. The speed-up for the total calculation is with seven Laplace grid points a factor of five. With five grid points the speed-up increases to a factor of seven and with four grid points even to almost a factor of nine.

For ADC(2) the determination of the ground state amplitudes and the respective Lagrange multipliers is not iterative and the Jacobian is symmetric, so that no left eigenvalue problem has to be solved. Therefore the SOS–ADC(2) method requires only about a third of the computational costs for the solution of the linear equation systems, which makes this method an attractive approach for the optimization of excited state structures.

Finally we applied the Laplace-transformed SOS–CC2 algorithm to the ditopic 2,2′:6′,2″-bis(terpyridine) T13 from Ref. [27], with the structure depicted in Fig. 4. This molecule is a candidate for the synthesis of supramolecular architectures. [27] It has 160 atoms and, using the TZVP basis set and freezing only occupied core orbitals, 241 active occupied and 1943 virtual orbitals and 6174 auxiliary basis functions for the RI approximation. We calculated the gradient for the lowest $\pi\pi^*$ excited state on seven processors with seven Laplace grid points, which leads to a small value of the Laplace error function of 3.6×10^{-8}. The wall time for the calculation of $D^{F,\xi}_{pq}(\bar{t}^{ex})$ was 6 h and 50 min. We estimated a speed-up of a factor of 6.7 for this density with the Laplace algorithm. The calculation of $D^{F,A}(\bar{E},E)$ took about 19 h and the estimated speed-

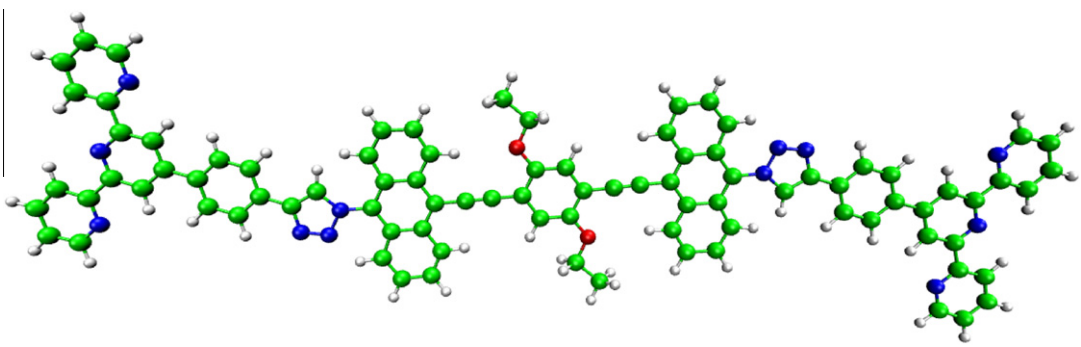


Fig. 4. Structure of the ditopic 2,2′:6′,2″-bis(terpyridine) T13 from Ref. [27].

Author's personal copy

up is a factor of 5.7. The solution of the linear equations needed about three days. For this part the Laplace algorithm is faster by a factor of seven for this system size and seven Laplace grid points. The speed-up for the whole calculation of a gradient for one excited state of T13 is a factor of seven with seven grid points. By deleting also virtual anti-core orbitals and relaxing the Laplace convergence to $F^{\mathrm{Lap}} \leqslant 10^{-4}$ only three grid points are used so that the speed-up increases to a factor of 16.

5. Summary

We presented a fourth order scaling algorithm for gradients of ground and excited states, excited state properties and transition moments in the framework of SOS–CC2 and SOS–ADC(2). With ADC(2) the determination of the ground state parameters and the Lagrange multipliers is not iterative and the Jacobian is symmetric, so that no left eigenvalue problem has to be solved. Since for CC2 most time during gradient and property calculations is spent on the iterative solution of the linear equation systems, the SOS–ADC(2) method provides significant savings compared to SOS–CC2. The derivation and computational timings for the densities are completely analogous to SOS–CC2. In combination with the parallel implementation these developments permit the calculation of spectra and the optimization of excited state structures for molecules with more than 150 atoms using standard computer hardware, which would be prohibitive with other correlated wavefunction methods.

We determined the error of the numerical Laplace transformation for adiabatic electronic excitation energies, excited state structure parameters and oscillator strengths. This Laplace error is for adiabatic excitation energies about one order of magnitude smaller than for vertical excitation energies. This is due to a fortunate error cancellation. Also for structure parameters, such as bond lengths and angles, as well as oscillator strengths the Laplace error is found to be very small.

We evaluated the accuracy of SOS–ADC(2) for adiabatic electronic excitation energies, structure parameters in the excited state, harmonic vibrational frequencies as well as dipole moments and oscillator strengths and compared to SOS–CC2 and unscaled CC2. As for vertical excitation energies, adiabatic excitation energies are blue shifted with SOS–ADC(2). For aldehydes SOS–ADC(2) excitation energies are less blue shifted than with SOS–CC2. We find that for excited state structures SOS–CC2 performs slightly better than unscaled CC2. Especially the overestimation of the C–O-bond length of aldehydes after $n\pi^*$ excitations is reduced with SOS–CC2. This improvement over CC2 is not seen for SOS–ADC(2), but the accuracy obtained with SOS–ADC(2) is still close to that of CC2. Since SOS–ADC(2) is, due to the smaller number of equations that need to be solved, computationally cheaper, it is an attractive method for the calculation of spectra and the optimization of excited state structures.

The savings in computational time of the Laplace-transformed SOS–CC2 algorithm is for excited state densities somewhat smaller than for the solution of linear equation systems. For a series of glycine polypeptides with a varying number of glycine units the crossing point, where both algorithms need the same computational time, occurs for the excited state density between five and six glycines, whereas for the ground state density and the solution of linear equations the crossing points are already reached at about four glycines. For standard applications most time is spent on the solution of the linear equation systems, so that the benefit of the fourth order scaling algorithm is dominated by the larger speed-up for this part. For the calculation of a gradient for one excited state the total speed-up is for chlorophyll a factor of five and for a ditopic 2,2′:6′,2″-bis(terpyridine) with 160 atoms a factor of seven, when seven grid points for the numerical Laplace transformation are used in each case. By reducing the number of grid points, so that the convergence criterion for the Laplace error function is only 10^{-4}, speed-ups of a factor of nine for chlorophyll and even a factor of 16 for the bis(terpyridine) can be achieved.

References

[1] C. Hättig, J. Chem. Phys. 118 (17) (2003) 7751.
[2] A. Köhn, C. Hättig, J. Chem. Phys. 119 (10) (2003) 5021.
[3] C. Hättig, O. Christiansen, P. Jørgensen, J. Chem. Phys. 108 (20) (1998) 8331.
[4] C. Hättig, A. Köhn, J. Chem. Phys. 117 (15) (2002) 6939.
[5] R.C. Lochan, Y. Shao, M. Head-Gordon, J. Chem. Theor. Comput. 3 (2007) 988.
[6] Y.M. Rhee, D. Casanova, M. Head-Gordon, J. Chem. Theor. Comput. 5 (2009) 1224.
[7] A. Hellweg, S.A. Grün, C. Hättig, Phys. Chem. Chem. Phys. 10 (2008) 1.
[8] D. Kats, M. Schütz, J. Chem. Phys. 131 (2009) 124117.
[9] K. Freundorfer, D. Kats, T. Korona, M. Schütz, J. Chem. Phys. 133 (2010) 244110.
[10] N.O.C. Winter, C. Hättig, J. Chem. Phys. 134 (2011) 184101.
[11] A development of University of Karlsruhe and Forschungszentrum Karlsruhe GmbH, 1989–2007, Turbomole GmbH, Since 2007. Available from: <http://www.turbomole.com>, TURBOMOLE V6.3, 2011.
[12] Y. Jung, R.C. Lochan, A.D. Dutoi, M. Head-Gordon, J. Chem. Phys. 121 (20) (2004) 9793.
[13] O. Christiansen, P. Jørgensen, C. Hättig, Int. J. Quantum Chem. 68 (1998) 1.
[14] O. Vahtras, J. Almlöf, M.W. Feyereisen, Chem. Phys. Lett. 213 (1993) 514.
[15] O. Christiansen, A. Halkier, H. Koch, P. Jørgensen, T. Helgaker, J. Chem. Phys. 108 (7) (1998) 2801.
[16] R.F. Fink, J. Chem. Phys. 133 (2010) 174113.
[17] C. Hättig, Adv. Quantum Chem. 50 (2005) 37.
[18] J. Schirmer, Phys. Rev. A 26 (1982) 2395.
[19] J. Almlöf, Chem. Phys. Lett. 181 (1991) 319.
[20] M. Häser, J. Almlöf, J. Chem. Phys. 96 (1992) 489.
[21] M. Häser, Theor. Chim. Acta 87 (1993) 147.
[22] T.H. Dunning, J. Chem. Phys. 90 (1989) 1007.
[23] R.A. Kendall, T.H. Dunning, R.J. Harrison, J. Chem. Phys. 96 (1992) 6796.
[24] F. Weigend, A. Köhn, C. Hättig, J. Chem. Phys. 116 (2002) 3175.
[25] Downloaded from: <https://bse.pnl.gov/bse/portal>.
[26] The ratio of $\frac{32}{5}\frac{N_l}{N_o}$ proposed in J. Chem. Phys. 134, 184101 (2011) was incorrect.
[27] A. Wild, C. Friebe, A. Winter, M.D. Hager, U.-W. Grummt, U.S. Schubert, Eur. J. Org. Chem. 2010 (2010) 1859.
[28] K.P. Huber, G. Herzberg, Molecular Spectra and Molecular Structure: IV. Constants of Diatomic Molecules, Van Nostrand Reinhold, New York, 1979.
[29] K.P. Huber, G. Herzberg, Molecular Spectra and Molecular Structure: III. Electronic Spectra and Electronic Structure of Polyatomic Molecules, Van Nostrand Reinhold, New York, 1966.
[30] D.J. Chlouthier, D.A. Ramsay, Annu. Rev. Phys. Chem. 34 (1983) 31.
[31] T.R. Huet, M. Godefroid, M. Herman, J. Mol. Spectrosc. 144 (1990) 32.
[32] J.M. Hollas, Molecular structure from rotational and vibrational transitions in electronic spectra, in: R. Fausto (Ed.), Recent Experimental and Computational Advances in Molecular Spectroscopy, Kluwer, Dordrecht, 1993, p. 27.
[33] M. Izuha, K. Yamanouchi, J. Chem. Phys. 109 (1998) 1810.
[34] R.Y. Dong, R. Nanes, D.A. Ramsay, Rotational analyses of bands of the $\tilde{A}^1b_1 - \tilde{X}^1a_1$ system of cis-glyoxal, Can. J. Chem. 71 (1993) 1595.